NASA TECHNICAL MEMORANDUM

NASA TM X-73529

NASA TM X-73529

OTW NOISE CORRELATION FOR SEVERAL NOZZLE/WING GEOMETRIES USING A 5:1 SLOT NOZZLE WITH EXTERNAL DEFLECTORS

by U. von Glahn and D. Groesbeck
Lewis Research Center
Cleveland, Ohio 44135

TECHNICAL PAPER to be presented at the
Ninety-second Meeting of the Acoustical
Society of America
San Diego, California, November 16-19, 1976

OTW NOISE CORRELATION FOR SEVERAL NOZZLE/WING GEOMETRIES USING A 5:1 SLOT NOZZLE WITH EXTERNAL DEFLECTORS

by U. von Glahn and D. Groesbeck

Lewis Research Center

ABSTRACT

Acoustic spectral data obtained from a model-scale study of several OTW configurations with a 5:1 slot nozzle using various external deflectors are correlated in terms of deflector geometry and flow parameters. Variations in the deflector geometry include deflector size and deflector angle. In addition, geometry variations in flap setting and nozzle chordwise location are included. Three dominant noise sources are correlated: fluctuating lift noise, flap trailing edge noise, and jet mixing noise. Aerodynamic characteristics, including lift and thrust measurements, obtained for the various configurations are summarized.

E-8949

INTRODUCTION

The design of the exhaust nozzle shape for STOL engine over-the-wing (OTW) configurations has conflicting requirements for cruise and powered lift operation. For cruise, a small nozzle boattail angle ($<10^{o}$) is required in order to minimize the engine nacelle cruise-drag. On the other hand, a large internal nozzle angle, which can result in a large nacelle boattail angle, is needed in order to direct the jet exhaust flow toward the wing/flap surface and provide the flow attachment necessary for powered lift. Furthermore, in the powered-lift mode, a nozzle exhaust flow area about 20-percent larger than that for the cruise mode is needed for optimum engine performance. A solution to these design problems can be obtained by the use of a retractable external deflector shown schematically in figure 1. In the cruise mode, such a deflector would constitute a part of the exhaust nozzle while in the powered-lift mode the deflector would be extended to provide exhaust flow attachment to

the wing/flap surface and at the same time provide the necessary exhaust area modulation.

As has been shown in references 1 to 5, the use of external deflectors causes an increase in the configuration noise level due to exhaust flow interactions with the deflector and the wing/flap surfaces. In the present paper, representative acoustic spectra obtained from an exploratory model-scale study of several OTW configurations using a 5:1 aspect ratio slot nozzle with various external deflectors (ref. 5) are correlated in terms of external deflector geometry and flow parameters. Variations in the deflector geometry include deflector size and deflector angle relative to the nozzle centerline. In addition, geometry variations in flap setting and chordwise location of the nozzle are included. In order to provide for valid acoustic comparisons between alternate methods of providing flow attachment for powered lift, the aerodynamic characteristics, taken from reference 6, for the present nozzle/wing configurations are included.

APPARATUS AND PROCEDURE

Facility

The aerodynamic and acoustic data used herein were obtained using an out-of-doors facility within the 7×15 m courtyard of a subsonic wind tunnel at the Lewis Research Center. This facility is described in reference 7. Open-cell foam pads were used to minimize reflections from the surrounding walls and ground.

Sound pressure level (SPL) spectra were obtained using a 1.27-cm diameter condenser microphone with wind screen. Data were recorded at 90° to the jet axis at a microphone distance of 3.05 meters. The noise data were recorded on a FM tape recorder and digitized by a four second time averaged one-third octave band spectrum analyzer. The analyzer determined sound pressure level spectra in decibels referenced to 2×10^{-5} N/m^2.

Jet velocity profiles were obtained at the trailing edge of the shielding surfaces. Measurements were made with a traversing pitot tube with an

entrance cone angle of 60° to help minimize flow angularity effects resulting from the jet flow over the curved surfaces. A vane on the traversing probe was used to establish the jet flow angle for each traverse. When the flow angle, as determined by means of the vane, exceeded the angularity capability of the pitot tube, the tube angle to the local flow was adjusted to provide suitable data. The pressures measured were transmitted to an x-y-y' plotter which yielded direct traces on graph paper of the total pressure distribution across the jet.

Acoustic data were taken at nominal jet velocities of 198 and 261 m/sec. The lift-thrust measurements were made with nominal jet velocities of 195 and 253 m/sec while the flow contours at the trailing edge were obtained with a jet velocity of 253 m/sec.

Models

Nozzle. - A simple 5:1 slot nozzle (ref. 5) was used with various external deflectors to turn the flow (fig. 2). Each of the sides of the nozzle converged at 5° and the nominal nozzle dimensions at the exhaust plane were 2.0 centimeters by 10.2 centimeters. The overall external deflector dimensions are also given in figure 2. In general, the 40° full-lip deflector was similar to that used with the "D-nozzle" in reference 4.

Wing. - The wing used in the present tests was the same as the baseline wing of reference 5 and is shown in figure 3 together with pertinent dimensions. The surface consisted of a metal plate secured to wooden ribs. The surface approximated the upper surface contour of the airfoil with 20° and 60° deflected flaps used in references 1 and 2. The wing had a span of 61 centimeters. The nozzle was located at two axial locations on the surface (l-dimension in fig. 3) corresponding to nominal airfoil chordwise stations of 21- and 46-percent with flaps retracted. The chord of the wing with retracted flaps was 33 cm.

Data Normalization

The analysis of reference 8 indicated that the magnitudes of the several noise sources identified were a function of the measured shear layer height, δ_e. The term δ_e, obtained from the trailing edge Mach number contours (see appendix A), is defined as the shear layer height of the free jet boundary measured at the trailing edge where the local velocity is 0.5 that of the local peak velocity, U_m. The measured shear layer height is corrected for the weight flow ratio, W/W_i as discussed in reference 8. For the present nozzle, the characteristic normalized height, δ^*, is given by $\delta_e + h\sqrt{W_i/W - 1}$. Similarly, the normalized nozzle height, h^*, (see ref. 8) is given by $h\sqrt{W_i/W}$.

AERODYNAMIC RESULTS

Weight Flow Considerations

The ratios of the measured weight flow, W, to the ideal flow, W_i, for the nozzle with the external deflectors and no wing are given in table I. The measured weight flow in all cases is within 1.1% of the ideal. This reduction in weight flow contrasts with up to nearly 10% for the 5:1 slot nozzle alone configurations of reference 6.

Also given in table I are the W/W_i ratios for the nozzle with external deflectors and including the wing/flap system. The data all indicate a reduction in weight flow due to both the deflector and wing/flap system of less than 10%. This, in turn, compares with reductions of, in some cases, over 20 percent for the 5:1 slot nozzle/wing configurations of reference 6 for a similar wing geometry. The flow reductions in the present study generally increase with increases in the nozzle chordwise location, deflector lip size, and flap setting. The limited range of the variables are insufficient to provide a general equation for prediction of weight flow reduction due to the deflector/wing geometry.

The preceding data indicate that the selected location of the external deflector relative to the nozzle exhaust plane affects the weight flow and that the deflector lip should perhaps be located further downstream of the nozzle exhaust plane for the case of plate-type deflector used herein. Use of a vane-type deflector, such as that used in reference 9 would possibly eliminate the back-pressure effect of the deflector on the nozzle weight flow.

Lift and Thrust Characteristics

In order to provide meaningful comparisons of the aerodynamic data, all configurations are compared on the basis of equal weight flow. This, of course, does not imply equal lift and thrust.

In order to achieve equal weight flow, the nozzle area must be increased, which would constitute a larger external wetted surface area resulting in a cruise-drag penalty. The latter consideration is beyond the scope of this study. The measured values of the static lift and thrust are normalized by compensating for the weight flow reductions caused by the nozzle/deflector configurations and the presence of the wing, as in reference 6. The adjusted measured static lift and thrust are then ratioed to the ideal nozzle-alone thrust. These procedures led to the following expressions for the normalized lift and thrust: $L_T(W_i/W)T_i$ and $T(W_i/W)T_i$, respectively. The normalized data in the form are shown in figure 4. The flow turning angle shown is that made by the flow with respect to the nozzle axis and is given by $\tan^{-1}(L_T/T)$. The magnitude of the vector sum of the lift and thrust, given by the magnitude of the radius in figure 4, represents a flow turning efficiency.

The data shown in figure 4 were taken from reference 6 and are included herein for completeness of the data presentation. Also shown in figure 4 (shaded regions) are the data ranges of the slot-nozzle/wing configurations from reference 6. These slot nozzles had internal roof angles (β) and were tested with and without nozzle sidewall cutback (γ). In general, the flow turning efficiency increases with reductions in deflector lip size and angle for the geometries included. The absolute efficiency values with the

external deflector configurations are less (up to 10 percentage points) than those for the comparable slot nozzle configurations of reference 6; however, the present configurations are not considered to be optimum geometries. In all cases the external deflectors provided larger turning angles (2° to 8°) than those with the slot nozzles.

Trailing Edge Velocity Profiles

From Mach number contour plots made normal to the flap trailing edge (see appendix A), velocity profiles were developed at the nozzle centerline. The resulting velocity profiles were normalized by the ratio δ/δ_e and M_l/M_p as shown in figure 5. For each flap setting in figure 5, the shape of the normalized velocity profile is independent of deflector size and deflector angle. The shape of the profiles are similar in most respects to those for the 5:1 slot nozzle/wing configurations of reference 6.

The most significant difference between the present work and that for the 5:1 slot nozzle/wing configurations of reference 6 is for the 60° flap setting. The present velocity profiles indicate reasonably good flow attachment to the surface whereas the 5:1 slot nozzles/wings from reference 6 did not, as evidenced by low M_l/M_p values near the surface and location of the peak M_l/M_p at significantly higher δ/δ_e values than those with the present configurations.

An overall comparison of the profiles for flap deflections of 20° and 60° is also shown in figure 5(b). While the profile shapes are somewhat similar, the slope of the velocity profile curve at the free shear layer is steeper for the 20° flap angle than that for the 60° flap angle.

Although the velocity profile shapes on a nondimensional basis are similar, the dimensional profiles associated with various nozzle/wing configurations are significantly different as shown in figure 6. The configurations shown in figure 6 are selected for each flap setting at substantially similar lift/thrust values (see fig. 4). At both flap settings the shear layer thicknesses with the 40/40 slot nozzle ($\beta = 40^{\circ}$, $\gamma = 40^{\circ}$; ref. 6) are thicker and the peak velocities higher than those with the external deflector. Further-

more, as expected, with the nozzles at the shorter chord location (21%), the profiles are thicker and the peak velocities are reduced compared with those at the longer chord location (46%).

Jet Velocity Decay

The peak jet velocity decay measured at the trailing edge of the present configurations is shown in figure 7 for both the 20° and 60° flap settings. The data were obtained on the nozzle centerline plane for an M_j of 0.8. The data are shown in terms of the ratio of M_p/M_j as a function of $L/D_e \sqrt{1 + M_j}$. The curves drawn through the data are similar in shape to those for the 5:1 slot nozzle/wing configurations in reference 6. As is apparent in figure 7, the ratio M_p/M_j decreases with an increase in $L/D_e \sqrt{1 + M_j}$ and with increases in deflector size and deflector angle. Also, the ratio M_p/M_j is somewhat less for a given configuration with a 60° flap setting than that with a 20° flap setting.

The peak jet velocity decay data range for the 5:1 slot nozzle/wing configurations (ref. 6) is also shown in figure 7 (shaded regions) for comparison with the present data. In all cases the configurations with external deflectors show a lower ratio of M_p/M_j than those for the configurations of reference 6 at a given value of $L/D_e \sqrt{1 + M_j}$.

CORRELATION OF SOURCE NOISE

Typical spectra for the nozzle/wing configurations with the various external deflectors are shown in figure 8 for a jet exhaust Mach number of 0.8. Also shown for comparison are spectra for the 30/30 slot nozzle configuration ($\beta = 30^{\circ}$, $\gamma = 30^{\circ}$) from the study in reference 5. For the data shown, the SPL levels increase with a decrease in the deflector angle. For a constant deflector angle, the levels also increase with a reduction in the deflector lip size.

The shape of the spectra for the external deflector configurations are similar to those for the 30/30 slot nozzle configuration. It should be noted that in the mid-frequencies (500 to 5000 Hz) the 30/30 slot nozzle configuration was noisier (2-5 dB) than the present configurations.

As in reference 8 three primary noise source regions are identified. These regions are shown schematically in figure 9 and consist of fluctuating lift noise (I), trailing edge noise (II), and a redirected jet mixing noise source that includes the noise caused by reflections of acoustic waves from the wing/flap surface (III). Also shown, for comparison, is a curve representing the spectrum for the nozzle-alone noise. A brief discussion of the characteristics of these noise sources is given in reference 8.

In the present paper, the noise sources are assumed uncorrelated and the measured SPL is the anti-logarithmic sum of the noise levels from all the noise sources. Independent correlations were developed for the peak SPL values of each of the noise sources shown in figure 9 in terms of the prime geometry and flow variables. The latter include the peak jet flow velocity at the flap trailing edge, a characteristic dimensions, jet exhaust velocity, and nozzle geometric variables such as, in the present case, deflector lip angle, and deflector size.

In the correlation of the acoustic data for the several noise sources associated with the present configurations, the open sides (spanwise direction) of the deflector were assumed to constitute a cutback angle, γ, of 90^{o}. The nozzle height, corrected for weight flow reduction, was taken at the nozzle exhaust plane. An alternate approach would have been to assume the characteristic nozzle height to be the dimension between the deflector lip and wing surface. However, this dimensional consideration was accounted for in the present analysis by the deflector lip immersion ratio, I_m/I_{m_T} (see table II for I_m/I_{m_T} values). The nozzle roof angle used in the correlation of reference 8 was considered herein to be the same as the deflector lip angle, i.e., β.

Noise Source I - Fluctuating Lift Noise

The correlation of noise source I (fluctuating lift noise) was accomplished in reference 8 with 5:1 aspect ratio slot nozzles having a variety of nozzle roof (kickdown) angles and with and without nozzle sidewall cutback. The correlation curve is shown in figure 10(a) for flap settings of 20° and 60°. Also shown in the figure are the data obtained in the present work with the 5:1 aspect ratio slot nozzle using external deflectors in order to achieve powered lift. The ordinate in figure 10(a), as in reference 8, is given by the following relationship:

$$SPL^{*}_{I,p} = SPL_{I,p} + 10\,m \log \frac{U_j}{U_m} + 10 \log \frac{W_i}{W} - 40 \log U_j - 10 \log A \qquad (1)$$

where

$$m = 10 - 4\left[1 + 0.5\left(\frac{1}{1 + \frac{0.1}{M_j^8}}\right)\right] \qquad (2)$$

For the data herein, m = 5.70 and 4.72 for M_j values of 0.602 and 0.803, respectively.

The abscissa in figure 10(a) consists of: (1) the characteristic normalized shear layer height, δ^{*}; (2) the normalized nozzle height, h^{*}; and (3) terms accounting for the external deflector angle, β. The term accounting for the nozzle sidewall cutback angle, γ, with the external deflectors used reduces to a constant value of 2.0 for the present configuration ($1 + \sin^3\gamma = 2.0$, where $\gamma = 90^{\circ}$). From figure 10(a) it is apparent that the present data generally plot at higher $SPL^{*}_{I,p}$ values than that represented by the curve from reference 8. Also, the data for the 40° half-lip deflector lies below that for the full-lip deflector. The present data trend has the same slope exponent as that in reference 8; namely, a 4-power exponent.

Examination of the data led to the inclusion of a deflector lip immersion ratio, I_m/I_{m_T}. This term accounts for the immersion of the deflector lip into

the nozzle exhaust flow. It adjusts, in a sense, the nozzle height from the nozzle exhaust plane to the trailing edge of the deflector lip. Correlation of $SPL^*_{I,p}$ in terms of the abscissa parameters given in figure 10(a) and the deflector-lip immersion parameter, $\left(1 + (I_m/I_{m_T})^2\right)^2$ is shown in figure 10(b). The solid curve, included in the figure for comparison, represents the slot nozzle configurations of reference 8. (The ratio I_m/I_{m_T} for the reference 8 configurations is zero because no deflector was used.) The present data for noise source I correlate well, particularly with a 20^o flap setting, with these parameters and on the same curve as the data in reference 8.

With a 60^o flap setting, the data deviate from the correlation curve in much the same manner as those in reference 8. The lack of correlation for the 40^o half-lip deflector with a 60^o flap setting is again believed due to the partial separation of the flow from the surface at the 60^o flap setting as discussed in appendix A and also in reference 8.

Noise Source II - Trailing Edge Noise

The present data for noise source II are presented in figure 11(a) in terms of the correlation parameters developed in reference 8. Also shown for comparison is the correlation curve for the slot nozzle configurations from this reference. The ordinate is given by:

$$SPL^*_{II,p} = SPL_{II,p} + 10 \log \frac{W_i}{W} + 50 \log \frac{U_j}{U_m} - 80 \log U_j - 10 \log A \qquad (3)$$

while the abscissa is given by δ^*/h^*. It is obvious from figure 11(a) that the preceding parameters do not correlate the present data. The data trends, as plotted in figure 11(a), indicate a higher slope than that in reference 8 and a dependency on flap setting.

Because of the limited range of the data, several possible correlations were examined before a final arbitrary selection was made. All the correlations had a common basis; namely that the measured noise source II was

a composite of noise (anti-logarithmic sum) due to the flow over the trailing edge and the deflector. Consequently, the trailing edge noise correlation for the slot nozzle was separated out of the measured noise level by assuming that the trailing edge noise was represented by the correlation of reference 8. The remaining trailing edge noise attributed to the deflector was then analyzed and correlated. The result of this data correlation is shown in figure 11(b). The ordinate in figure 11(b) is given by:

$$SPL^{*}_{II\text{-}D,p} = SPL_{II\text{-}D,p} + 10 \log \frac{W_i}{W} + 40 \log \frac{U_j}{U_m} - 80 \log U_j - 10 \log A \quad (4)$$

Also, the abscissa is given by $\delta^*/h^* (1 + \sin^2\alpha)^{-1} (I_m/I_{m_T})$. These correlation terms yield a 1-power slope or exponent as indicated in figure 11(b). Note that the exponent of U_j/U_m in equation (3) is reduced from 5 to 4 in equation (4). The effect of flap setting noted for figure 11(a) is accounted for by the inclusion of the α-function in figure 11(b). The deflector-lip immersion ratio (I_m/I_{m_T}) correlates the full-lip with the half-lip deflector data.

Thus, the total peak noise source II level is obtained from the anti-logarithmic sum of the nozzle associated flow noise at the trailing edge obtained from equation (3) and the curve in figure 11(a) or reference 8 and the deflector associated flow noise at the trailing edge obtained from equation (4) and the curve shown in figure 11(b). Note that when I_m/I_{m_T} is zero (no deflector), the level of noise source II is that given in reference 8 for slot nozzles.

Noise Source III - Jet Mixing Noise

The data for noise source III are presented in figure 12(a) in terms of the correlation parameters developed in reference 8 for slot nozzle configurations. Also shown in the figure is the correlation curve for the slot nozzle configurations from this reference. The ordinate is given by:

$$SPL^{*}_{III,p} = SPL_{III,p} + 40 \log \frac{U_j}{U_m} + 10 \log \frac{W_i}{W} - 80 \log U_j$$

$$- 10 \log A + 20 \log (1 + \sin^2 \alpha) \qquad (5)$$

while the abscissa consists of δ^*/h^* with appropriate geometry parameters as indicated in the figure. As in the case of noise source II, the present data are not correlated by the parameters developed for the slot nozzle configurations in reference 8.

Consequently, the data were analyzed on the basis that the measured data for noise source III with the external deflector configurations also consisted of the anti-logarithmic sum of redirected jet mixing noise (due to the nozzle flow interaction with the wing/flap (ref. 8)) and deflector noise (due to the flow interaction with the deflector). The latter noise was correlated in terms of the parameters shown in figure 12(b) where:

$$SPL^{*}_{III\text{-}D,p} = SPL_{III\text{-}D,p} + 30 \log \frac{U_j}{U_m} + 10 \log \frac{W_i}{W} - 80 \log U_j - 10 \log A \quad (6)$$

and the abscissa is given by $\delta^*/h^* (2 - \cos\beta)(1 + \sin^2\alpha) I_m/I_{m_T}$. The data appear to be reasonably well correlated by these parameters. Again, as for the noise source II, the deflector associated noise source III becomes zero when I_m/I_{m_T} is zero (no deflector). The total peak noise source III level is obtained from the anti-logarithmic sum of the nozzle associated noise (obtained from eq. (5) and the curve from fig. 12(a) or ref. 8) and the deflector associated noise (obtained from eq. (6) and the curve from fig. 12(b)).

FREQUENCY AT PEAK SPL

As is evident from the spectral data shown in figure 8, as well as that obtained in the entire program, the peak frequencies associated with

the peak SPL values and the spectral shapes are substantially similar for slot nozzles with or without external deflectors provided the jet flow is attached to the wing/flap surfaces. Therefore, the relationships predicting these frequencies for noise sources I and II for slot nozzles also apply to the present configurations with external deflectors.. The spectral shapes for each of the noise sources given in reference 8 with slot nozzles also are valid for the present configurations.

The prediction of the acoustic spectra for the nozzle/deflector/wing configuration herein is procedurally similar to that given in reference 8. In this procedure, the noise sources are assumed uncorrelated and thus the total sound field can be approximated by summing anti-logarithmically the contributions of the various noise sources.

CONCLUDING REMARKS

The various jet and interaction noise sources associated with STOL engine over-the-wing configurations using a variety of 5:1 aspect ratio slot nozzles were correlated in terms of configuration related geometry and flow parameters in reference 8. Use of an external deflector for promoting jet flow attachment to the wing/flap surfaces requires additional analyses in order to include the effect of the deflector geometry on the previously identified noise sources. Because of the limited data available, several correlations could be obtained that provide a high and equal degree of data correlation. The final correlation parameters presented herein for the deflector associated noise were selected on the basis of the least variation from the parameters developed for slot nozzles in reference 8. Further work to verify the selection of these deflector parameters is needed. Finally, the noise levels of the present type of external deflector configurations having optimum aerodynamic characteristics remain to be established.

APPENDIX A

MACH NUMBER FLOW CONTOURS AT FLAP TRAILING EDGE

Mach number contour maps obtained normal to the flap trailing edge are shown for all the present external deflector configurations in figures 13 to 15 for a nominal jet exhaust Mach number of 0.8. The procedural details used in obtaining these contour maps are given in reference 5. From these maps, velocity profiles were developed at the flap trailing edge centerline. The latter were used to determine the δ^* and U_m values necessary for the aerodynamic parameters in the correlation of the acoustic data.

The present configurations all showed a large spanwise distribution of the nozzle flow at the flap trailing edge. Good attachment is apparent for nearly all the data shown. However, with a 60^o flap setting and the nozzle located at 21% chord, the location of the peak velocity (Mach number) was considerably farther away from the trailing edge surface than for all other configurations. From this it may be implied that some degree of flow separation from the flap is being encountered. In addition, the 40^o half-lip deflector for this operating condition, has a much thicker trailing edge shear layer (fig. 15) than the other configurations. This can also be interpreted as a further indication of some flow separation from the flap surface. As indicated in reference 6, limited visual flow studies confirmed these observations.

APPENDIX B

NOMENCLATURE

(All data are in SI units.)

A	nozzle exhaust area
D_e	equivalent nozzle diameter
h	measured nozzle height
h^*	normalized nozzle height
I_m	flap immersion into jet flow
l	wing chord length upstream of nozzle exhaust plane
L	shielding surface length
L_s	projected shielding length parallel to wing chordline
L_T	lift
M	Mach number
m	exponent defined in text (eq. (2))
SPL^*	normalized SPL, defined in text
SPL	measured sound pressure level, dB re 2×10^{-5} N/m^2
T	thrust
U	flow velocity
W	weight flow
Y, x, y, C, D	wing surface contour dimensions (see figs. 2 and 3)
α	flap setting (angle)
β	deflector or nozzle roof angle (ref. 8)
γ	nozzle sidewall cutback angle (ref. 8)
δ	local shear layer thickness at flap trailing edge

δ	shear layer thickness where $U = 0.5\, U_m$
δ^*	normalized shear layer thickness dimension at $U = 0.5\, U_m$
I, II, III	noise sources

Subscripts:

D	deflector
i	ideal
j	jet exhaust
ℓ	local
m	maximum
p	peak
T	total
I, II, III	noise sources

REFERENCES

1. M. Reshotko, W. A. Olsen, and R. G. Dorsch (1972). "Preliminary Noise Tests of the Engine-Over-the-Wing Concept. I. 30^{o}-60^{o} Flap Position," NASA TM X-68032.

2. M. Reshotko, W. A. Olsen, and R. G. Dorsch (1972). "Preliminary Noise Tests of the Engine-Over-the-Wing Concept. II. 10^{o}-20^{o} Flap Position," NASA TM X-68104.

3. M. Reshotko, J. H. Goodykoontz, and R. G. Dorsch (1973). "Engine-Over-the-Wing Noise Research," 6th Fluid and Plasma Dynamics Conference, Palm Springs, Calif., AIAA Paper 73-631.

4. M. Reshotko and R. Friedman (1973). "Acoustic Investigation of the Engine-Over-the-Wing Concept Using a D-Shaped Nozzle," Aero-Acoustic Specialists Conference, Seattle, Wash., AIAA Paper 73-1030.

5. U. von Glahn and D. Groesbeck (1975). "Geometry Effects on STOL Engine-Over-the-Wing Acoustics with 5:1 Slot Nozzles," NASA TM X-71820.

6. U. von Glahn and D. Groesbeck (1976). "Nozzle and Wing Geometry Effects on OTW Aerodynamic Characteristics," 12th Propulsion Conference, Palo Alto, Calif., AIAA Paper 76-622.

7. U. von Glahn and D. Groesbeck (1975). " Acoustics of Attached and Partially Attached Flow for Simplified OTW Configurations with 5:1 Slot Nozzle," NASA TM X-71807.

8. U. von Glahn and D. Groesbeck (1976). " OTW Noise Correlation for Variations in Nozzle/Wing Geometry with 5:1 Slot Nozzles," 3rd Aero-Acoustics Conference, Palo Alto, Calif., AIAA Paper 76-521.

9. U. von Glahn and D. Groesbeck (1976). "Effect of External Jet-Flow Deflector Geometry on OTW Aero-Acoustic Characteristics," 3rd Aero-Acoustics Conference, Palo Alto, Calif., AIAA Paper 76-499.

TABLE I. - CONFIGURATION WEIGHT FLOWS; $M_j = 0.8$

Deflector	Nozzle chordwise location, %	Ratio measured-to-ideal weight flow, W/W_i:	
		20^o Flap setting	60^o Flap setting
30^o Full lip	21	0.962	0.943
40^o Full lip	↓	.937	.911
40^o Half lip	↓	.956	.937
30^o Full lip	46	0.949	0.937
40^o Full lip	↓	.905	.918
40^o Half lip	↓	.949	.937
		W/W_i:	
30^o Full lip	No wing	0.989	
40^o Full lip	↓	.989	
40^o Half lip	↓	.998	

TABLE II. - DEFLECTOR LIP IMMERSION

IN JET STREAM

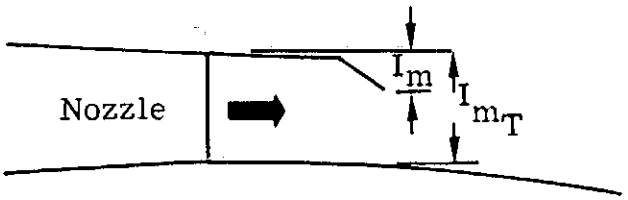

Deflector	Nozzle chordwise location, $\frac{c}{c}$	Flap setting, α, deg	I_{m_T}, cm	I_m/I_{m_T}
30^o Full lip	21	20	2.29	0.39
	46	20	2.39	.37
	21	60	2.36	.38
	46	60	2.41	.37
40^o Full lip	21	20	2.24	0.42
	46	20	2.34	.40
	21	60	2.34	.40
	46	60	2.36	.40
40^o Half lip	21	20	2.26	0.23
	46	20	2.29	.22
	21	60	2.34	.22
	46	60	2.44	.21

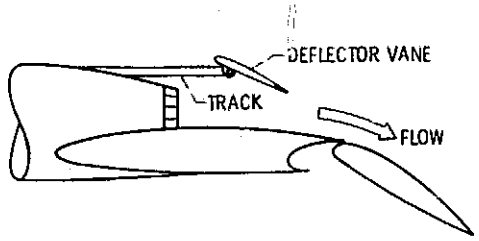

Figure 1. - Conceptual OTW nozzle-on-wing configuration with external deflector.

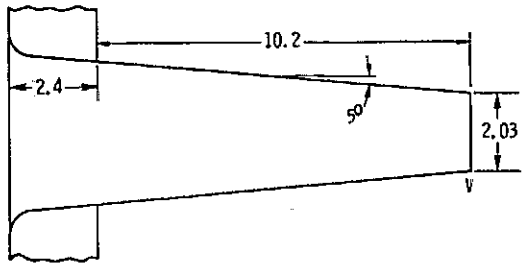

(a) 5:1 SLOT NOZZLE.

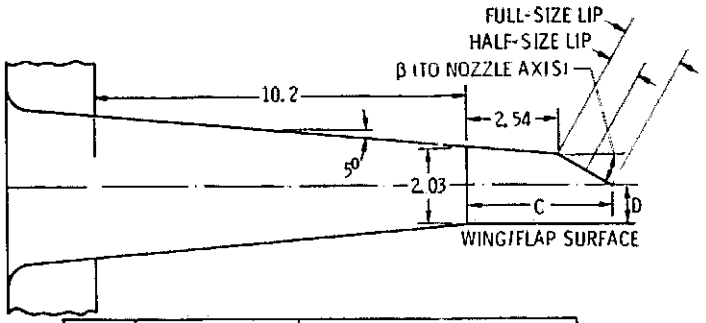

FLAP ANGLE, α, DEG	NOZZLE POSITION, % CHORD	DEFLECTOR ANGLE, θ					
		30°		40°- FULL LIP		40°- ½ LIP	
		C	D	C	D	C	D
20	21	4.0	1.40	3.63	1.30	3.20	1.75
	46	↓	1.50	↓	1.40	↓	1.78
60	21	↓	1.47	↓	1.40	↓	1.83
	46	↓	1.52	↓	1.42	↓	1.93

(b) DEFLECTOR DIMENSIONS WITH 5:1 SLOT NOZZLE. ALL DEFLECTORS WERE 15.2 CM WIDE.

Figure 2. - Sketches of test nozzle and external deflectors. Dimensions in centimeters.

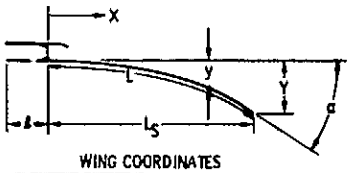

WING COORDINATES

FLAP ANGLE α, DEG	x/L_s / y/Y	0-0.4	0.5	0.6	0.7	0.8	0.9	0.95	0.975	1.0
20		0	0.04	0.13	0.26	0.44	0.70	0.85	-----	1.0
60		0	0.02	0.055	0.125	0.25	0.44	0.61	0.76	1.0

WING DIMENSIONS

FLAP ANGLE α, DEG	NOZZLE POSITION, % CHORD	Y, CM	Δ, CM	L_S, CM	L, CM
20	21	6.6	6.9	33.8	35.4
	46	6.6	15.2	25.4	27.0
60	21	14.3	6.9	30.5	38.7
	46	14.3	15.2	22.1	30.2

Figure 3. - Wing dimensions and coordinates. Dimensions in centimeters.

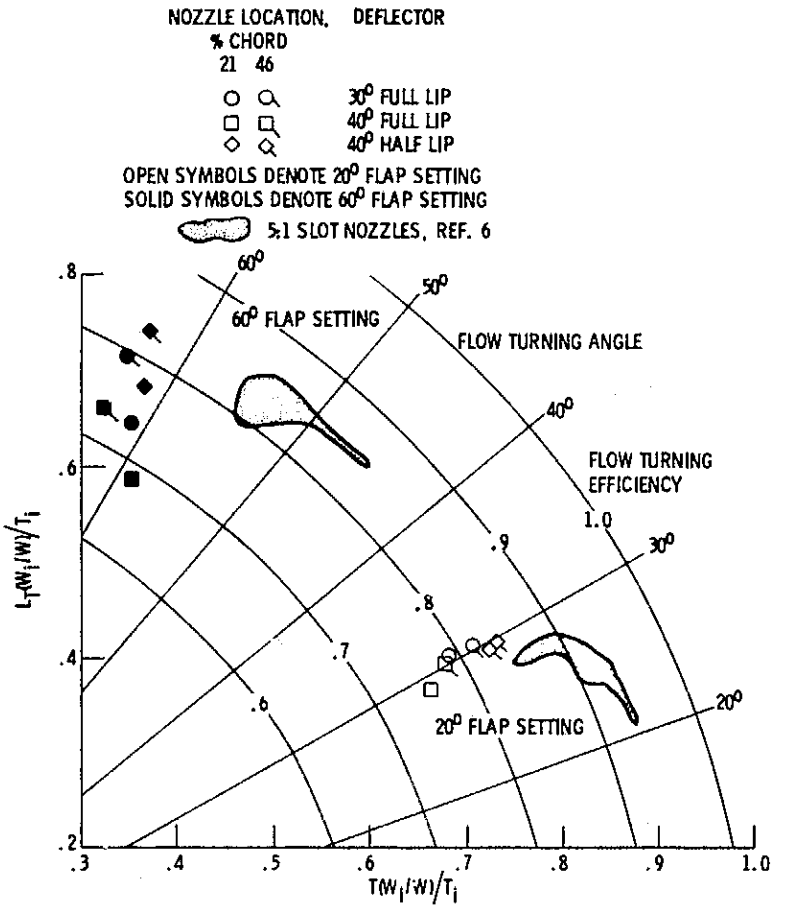

Figure 4. - Static turning effectiveness for various nozzle/wing configurations with external deflectors; M_j, 0.805.

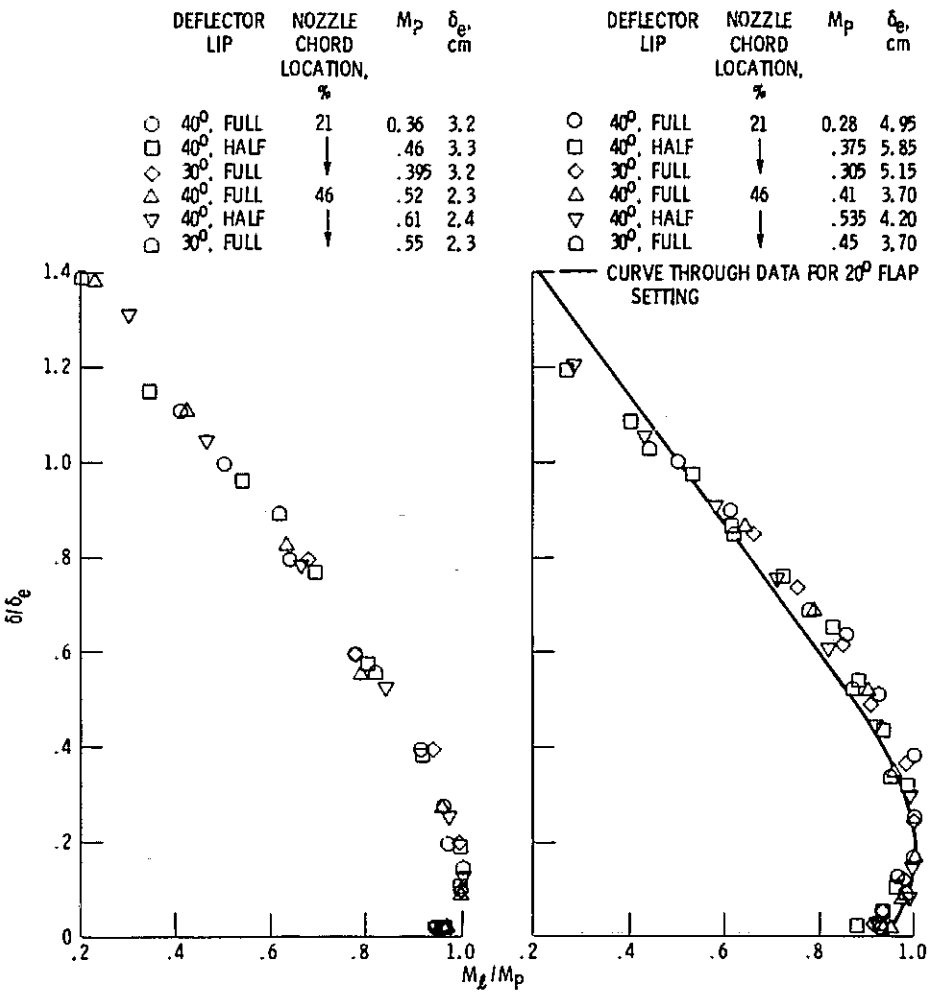

(a) 20° FLAP SETTING. (b) 60° FLAP SETTING.

Figure 5. - Normalized trailing edge velocity profiles at nozzle centerline; M_j, 0.8.

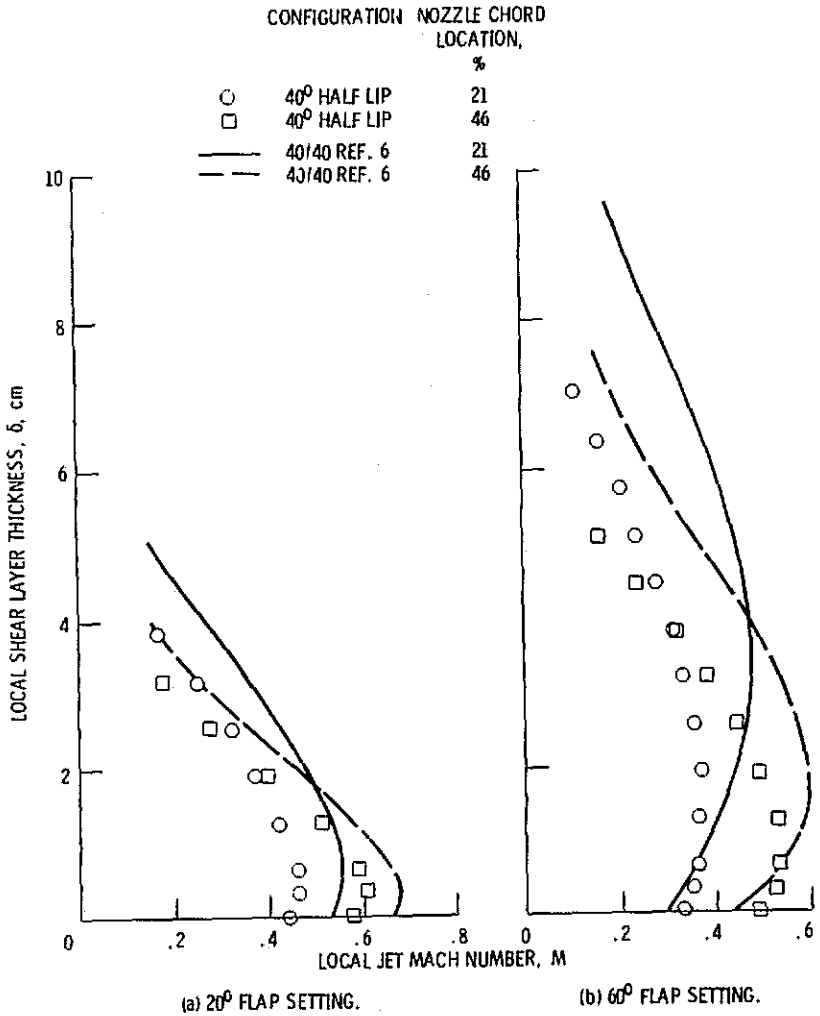

Figure 6. - Comparison of trailing-edge velocity profiles for 40° half-tip external deflector with those for 40/40 nozzle of reference 6; M_j, 0.8; lift/thrust approximately the same.

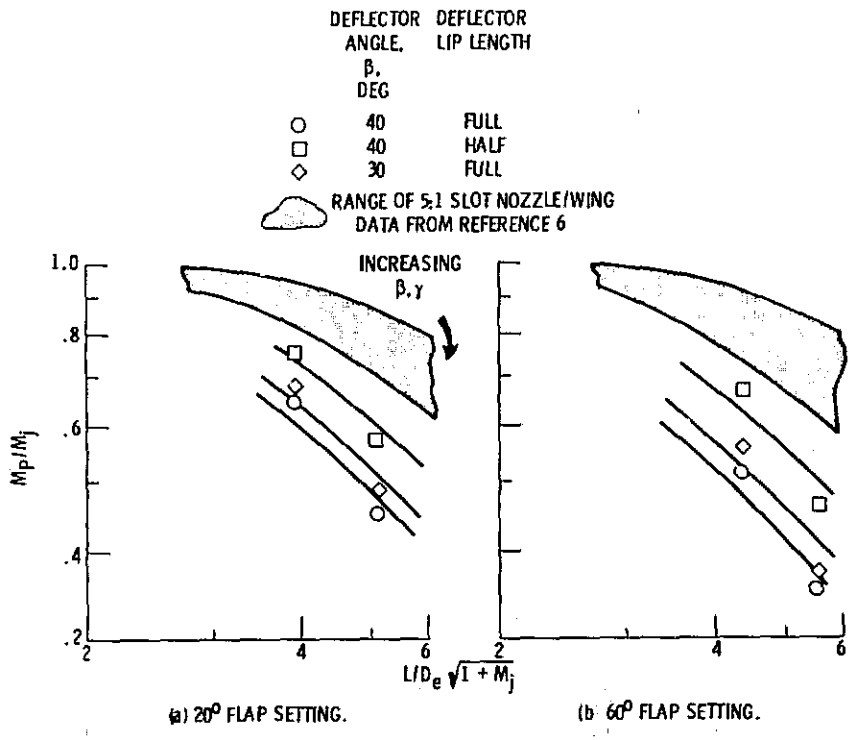

Figure 7. - Peak jet velocity decay at flap trailing edge for nozzle/wing configurations with external deflectors; M_j, 0.8.

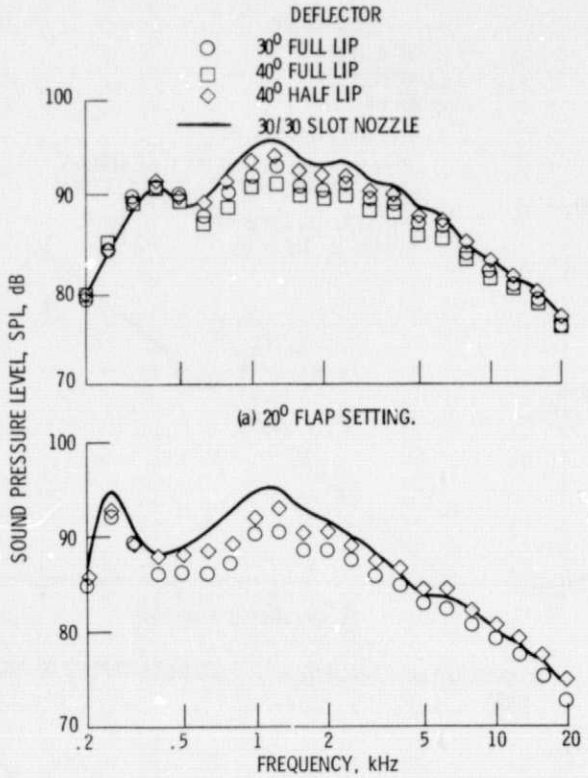

Figure 8. - Representative spectral comparison of external deflector configurations with 30/30 slot nozzle from reference 5; M_j, 0.8; nozzle at 21% chord.

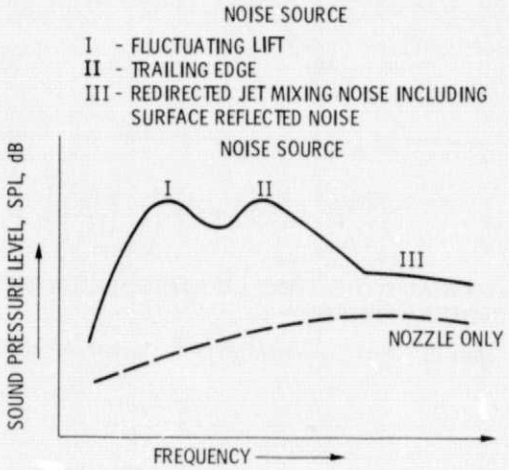

Figure 9. - Noise sources associated with OTW configurations.

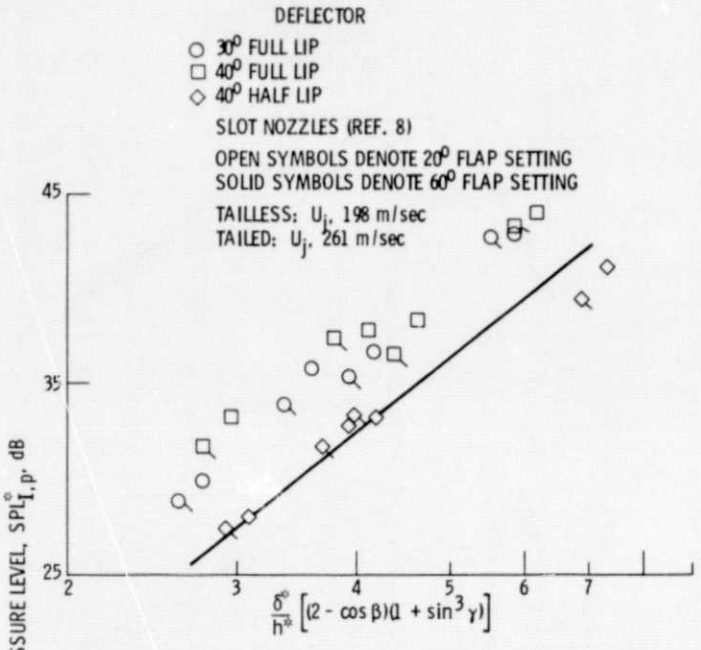

(a) CORRELATION PARAMETERS OF REFERENCE 8 APPLIED TO PRESENT DATA

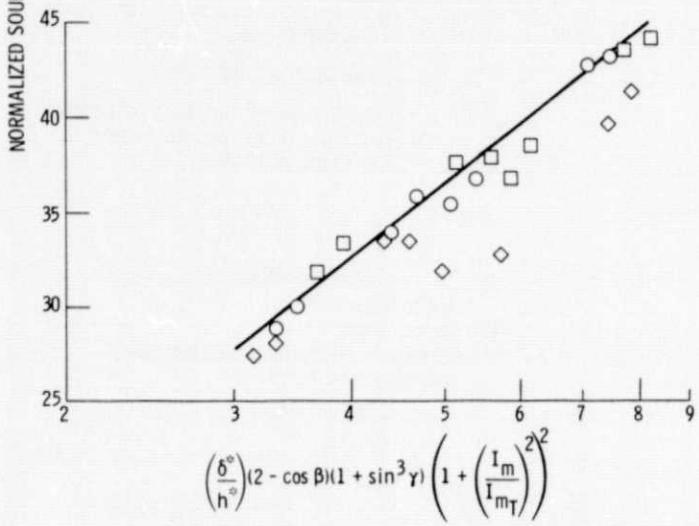

(b) CORRELATION OF REFERENCE 8 MODIFIED TO INCLUDE DEFLECTOR ASSOCIATED DIMENSIONS.

Figure 10. - Peak SPL correlation for fluctuating life noise source I.

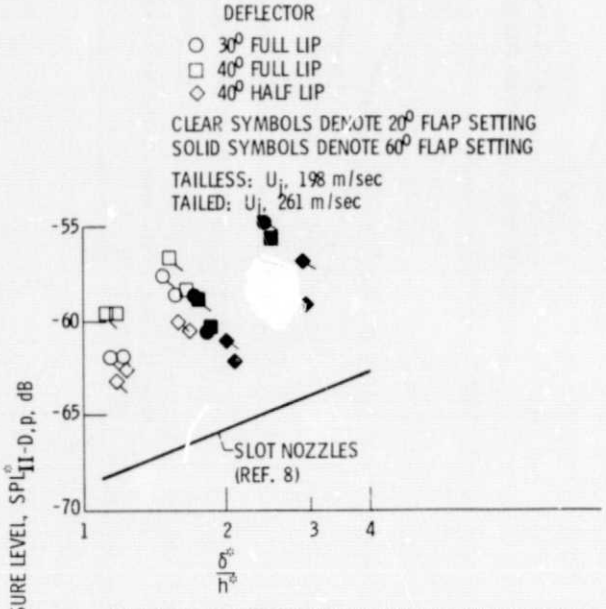

(a) CORRELATION PARAMETERS FROM REFERENCE 8 APPLIED TO PRESENT DATA.

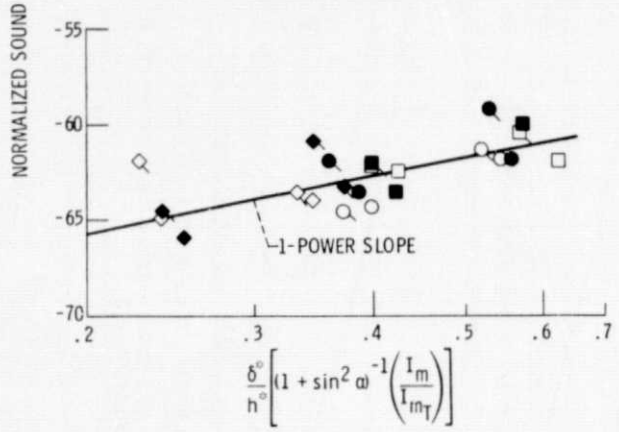

(b) CORRELATION OF DEFLECTOR NOISE SOURCE.

Figure 11. - Correlation of trailing edge related noise source II.

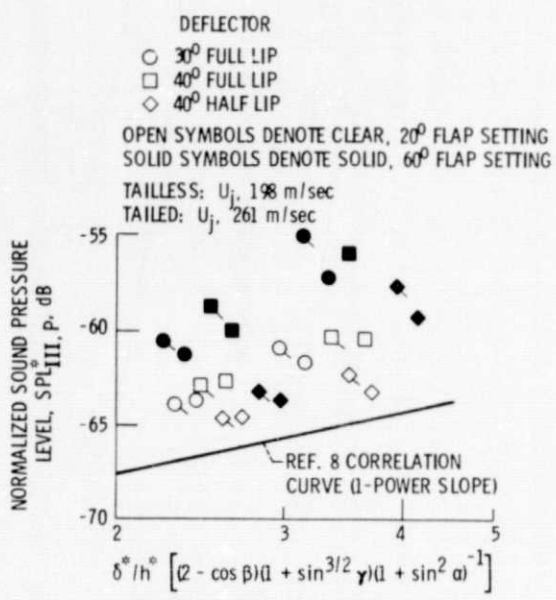

(a) CORRELATION PARAMETERS OF REF. 8 APPLIED TO PRESENT DATA.

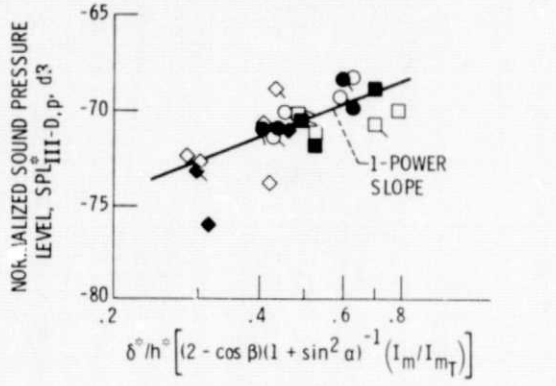

(b) CORRELATION OF MIXING NOISE RELATED TO DEFLECTOR.

Figure 12. - Correlation of peak SPL for mixing noise source III.

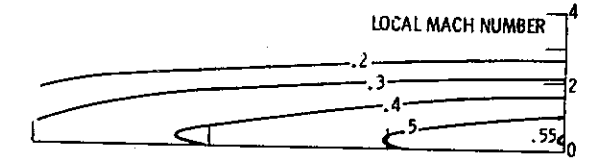

(a) 20° FLAP SETTING; NOZZLE AT 46% CHORD.

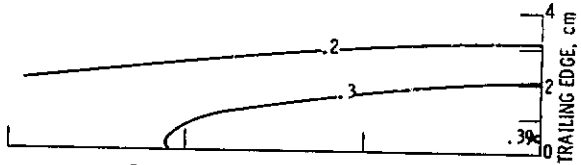

(b) 20° FLAP SETTING; NOZZLE AT 21% CHORD.

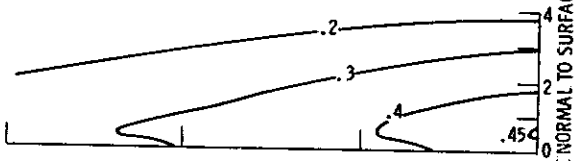

(c) 60° FLAP SETTING; NOZZLE AT 46% CHORD.

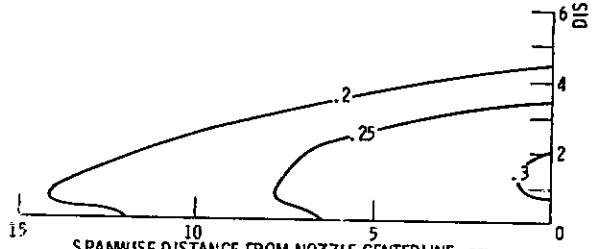

(d) 60° FLAP SETTING; NOZZLE AT 21% CHORD.

Figure 13. - Mach number contours at flap trailing edge with 30° full-lip deflector; M_j, 0.8.

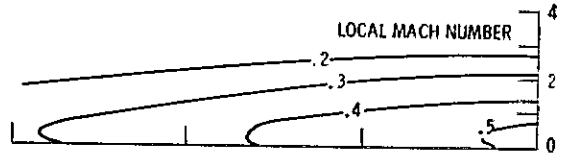

(a) 20° FLAP SETTING; NOZZLE AT 46% CHORD.

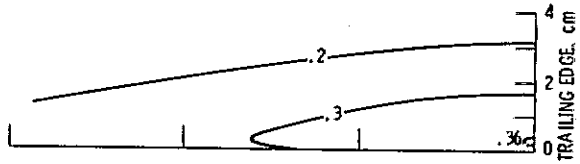

(b) 20° FLAP SETTING; NOZZLE AT 21% CHORD.

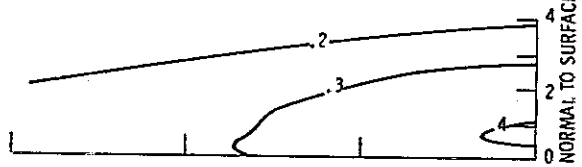

(c) 60° FLAP SETTING; NOZZLE AT 46% CHORD.

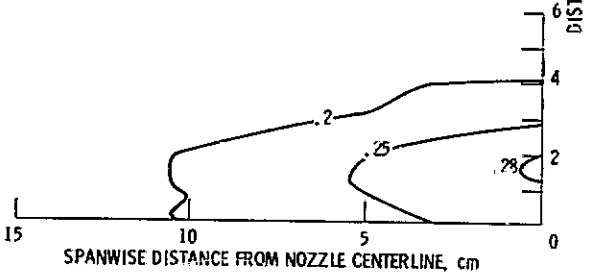

(d) 60° FLAP SETTING; NOZZLE AT 21% CHORD.

Figure 14. - Mach number contours at flap trailing edge with 40° full-lip deflector; M_j, 0.8.

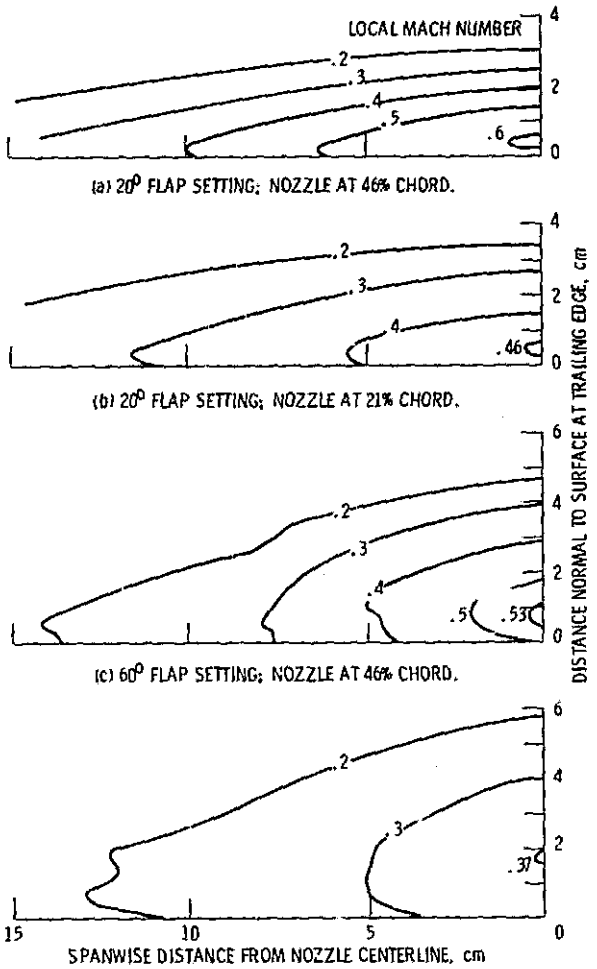

Figure 15. - Mach number contours at flap trailing edge with 40° half-lip deflector; M_j, 0.8.